This paper is published as part of a *PCCP* themed issue series on biophysics and biophysical chemistry:

Biomolecular Structures: From Isolated Molecules to Living Cells

Guest Editors: Seong Keun Kim, Jean-Pierre Schermann and Taekjip Ha

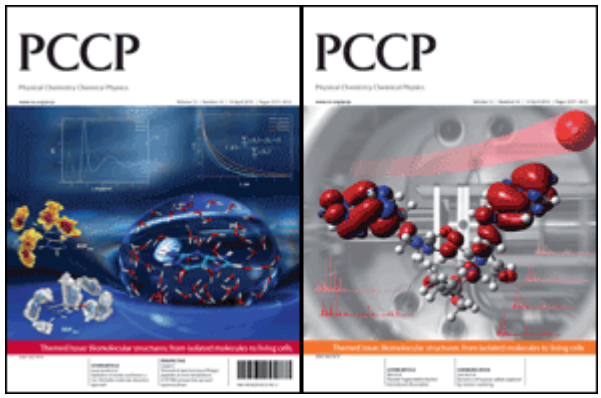

Editorial

Biomolecular Structures: From Isolated Molecules to the Cell Crowded Medium
Seong Keun Kim, Jean-Pierre Schermann, Taekjip Ha, *Phys. Chem. Chem. Phys.*, 2010
DOI: 10.1039/c004156b

Perspectives

Theoretical spectroscopy of floppy peptides at room temperature. A DFTMD perspective: gas and aqueous phase
Marie-Pierre Gaigeot, *Phys. Chem. Chem. Phys.*, 2010
DOI: 10.1039/b924048a

Communications

Dynamics of heparan sulfate explored by neutron scattering
Marion Jasnin, Lambert van Eijck, Michael Marek Koza, Judith Peters, Cédric Laguri, Hugues Lortat-Jacob and Giuseppe Zaccai, *Phys. Chem. Chem. Phys.*, 2010
DOI: 10.1039/b923878f

Papers

Infrared multiple photon dissociation spectroscopy of cationized methionine: effects of alkali-metal cation size on gas-phase conformation
Damon R. Carl, Theresa E. Cooper, Jos Oomens, Jeff D. Steill and P. B. Armentrout, *Phys. Chem. Chem. Phys.*, 2010
DOI: 10.1039/b919039b

Structure of the gas-phase glycine tripeptide
Dimitrios Toroz and Tanja van Mourik, *Phys. Chem. Chem. Phys.*, 2010
DOI: 10.1039/b921897a

Photodetachment of tryptophan anion: an optical probe of remote electron
Isabelle Compagnon, Abdul-Rahman Allouche, Franck Bertorelle, Rodolphe Antoine and Philippe Dugourd, *Phys. Chem. Chem. Phys.*, 2010
DOI: 10.1039/b922514p

A natural missing link between activated and downhill protein folding scenarios
Feng Liu, Caroline Maynard, Gregory Scott, Artem Melnykov, Kathleen B. Hall and Martin Gruebele, *Phys. Chem. Chem. Phys.*, 2010
DOI: 10.1039/b925033f

Vibrational signatures of metal-chelated monosaccharide epimers: gas-phase infrared spectroscopy of Rb^+-tagged glucuronic and iduronic acid
Emilio B. Cagmat, Jan Szczepanski, Wright L. Pearson, David H. Powell, John R. Eyler and Nick C. Polfer, *Phys. Chem. Chem. Phys.*, 2010
DOI: 10.1039/b924027f

Stepwise hydration and evaporation of adenosine monophosphate nucleotide anions: a multiscale theoretical study
F. Calvo and J. Douady, *Phys. Chem. Chem. Phys.*, 2010
DOI: 10.1039/b923972c

Reference MP2/CBS and CCSD(T) quantum-chemical calculations on stacked adenine dimers. Comparison with DFT-D, MP2.5, SCS(MI)-MP2, M06-2X, CBS(SCS-D) and force field descriptions
Claudio A. Morgado, Petr Jurečka, Daniel Svozil, Pavel Hobza and Jiří Šponer, *Phys. Chem. Chem. Phys.*, 2010
DOI: 10.1039/b924461a

Photoelectron spectroscopy of homogeneous nucleic acid base dimer anions
Yeon Jae Ko, Haopeng Wang, Rui Cao, Dunja Radisic, Soren N. Eustis, Sarah T. Stokes, Svetlana Lyapustina, Shan Xi Tian and Kit H. Bowen, *Phys. Chem. Chem. Phys.*, 2010
DOI: 10.1039/b924950h

Sugar–salt and sugar–salt–water complexes: structure and dynamics of glucose–KNO_3–$(H_2O)_n$
Madeleine Pincu, Brina Brauer, Robert Benny Gerber and Victoria Buch, *Phys. Chem. Chem. Phys.*, 2010
DOI: 10.1039/b925797g

Hydration of nucleic acid bases: a Car–Parrinello molecular dynamics approach
Alona Furmanchuk, Olexandr Isayev, Oleg V. Shishkin, Leonid Gorb and Jerzy Leszczynski, *Phys. Chem. Chem. Phys.*, 2010
DOI: 10.1039/b923930h

Conformations and vibrational spectra of a model tripeptide: change of secondary structure upon micro-solvation
Hui Zhu, Martine Blom, Isabel Compagnon, Anouk M. Rijs, Santanu Roy, Gert von Helden and Burkhard Schmidt, *Phys. Chem. Chem. Phys.*, 2010
DOI: 10.1039/b926413b

Peptide fragmentation by keV ion-induced dissociation
Sadia Bari, Ronnie Hoekstra and Thomas Schlathölter, *Phys. Chem. Chem. Phys.*, 2010
DOI: 10.1039/b924145k

Structural, energetic and dynamical properties of sodiated oligoglycines: relevance of a polarizable force field
David Semrouni, Gilles Ohanessian and Carine Clavaguéra, *Phys. Chem. Chem. Phys.*, 2010
DOI: 10.1039/b924317h

Studying the stoichiometries of membrane proteins by mass spectrometry: microbial rhodopsins and a potassium ion channel
Jan Hoffmann, Lubica Aslimovska, Christian Bamann, Clemens Glaubitz, Ernst Bamberg and Bernd Brutschy, *Phys. Chem. Chem. Phys.*, 2010
DOI: 10.1039/b924630d

Sub-microsecond photodissociation pathways of gas phase adenosine 5′-monophosphate nucleotide ions
G. Aravind, R. Antoine, B. Klærke, J. Lemoine, A. Racaud, D. B. Rahbek, J. Rajput, P. Dugourd and L. H. Andersen, *Phys. Chem. Chem. Phys.*, 2010
DOI: 10.1039/b921038e

DFT-MD and vibrational anharmonicities of a phosphorylated amino acid. Success and failure
Alvaro Cimas and Marie-Pierre Gaigeot, *Phys. Chem. Chem. Phys.*, 2010
DOI: 10.1039/b924025j

Infrared vibrational spectra as a structural probe of gaseous ions formed by caffeine and theophylline
Richard A. Marta, Ronghu Wu, Kris R. Eldridge, Jonathan K. Martens and Terry B. McMahon, *Phys. Chem. Chem. Phys.*, 2010
DOI: 10.1039/b921102k

Laser spectroscopic study on (dibenzo-24-crown-8-ether)–water and –methanol complexes in supersonic jets
Satoshi Kokubu, Ryoji Kusaka, Yoshiya Inokuchi, Takeharu Haino and Takayuki Ebata, *Phys. Chem. Chem. Phys.*, 2010
DOI: 10.1039/b924822f

Macromolecular crowding induces polypeptide compaction and decreases folding cooperativity
Douglas Tsao and Nikolay V. Dokholyan, *Phys. Chem. Chem. Phys.*, 2010
DOI: 10.1039/b924236h

Electronic coupling between cytosine bases in DNA single strands and *i*-motifs revealed from synchrotron radiation circular dichroism experiments
Anne I. S. Holm, Lisbeth M. Nielsen, Bern Kohler, Søren Vrønning Hoffmann and Steen Brøndsted Nielsen, *Phys. Chem. Chem. Phys.*, 2010
DOI: 10.1039/b924076d

Photoionization of 2-pyridone and 2-hydroxypyridine
J. C. Poully, J. P. Schermann, N. Nieuwjaer, F. Lecomte, G. Grégoire, C. Desfrançois, G. A. Garcia, L. Nahon, D. Nandi, L. Poisson and M. Hochlaf, *Phys. Chem. Chem. Phys.*, 2010
DOI: 10.1039/b923630a

Insulin dimer dissociation and unfolding revealed by amide I two-dimensional infrared spectroscopy
Ziad Ganim, Kevin C. Jones and Andrei Tokmakoff, *Phys. Chem. Chem. Phys.*, 2010
DOI: 10.1039/b923515a

Six conformers of neutral aspartic acid identified in the gas phase
M. Eugenia Sanz, Juan C. López and José L. Alonso, *Phys. Chem. Chem. Phys.*, 2010
DOI: 10.1039/b926520a

Binding a heparin derived disaccharide to defensin inspired peptides: insights to antimicrobial inhibition from gas-phase measurements
Bryan J. McCullough, Jason M. Kalapothakis, Wutharath Chin, Karen Taylor, David J. Clarke, Hayden Eastwood, Dominic Campopiano, Derek MacMillan, Julia Dorin and Perdita E. Barran, *Phys. Chem. Chem. Phys.*, 2010
DOI: 10.1039/b923784d

Guanine–aspartic acid interactions probed with IR–UV resonance spectroscopy
Bridgit O. Crews, Ali Abo-Riziq, Kristýna Pluháčková, Patrina Thompson, Glake Hill, Pavel Hobza and Mattanjah S. de Vries, *Phys. Chem. Chem. Phys.*, 2010
DOI: 10.1039/b925340h

Investigations of the water clusters of the protected amino acid Ac-Phe-OMe by applying IR/UV double resonance spectroscopy: microsolvation of the backbone
Holger Fricke, Kirsten Schwing, Andreas Gerlach, Claus Unterberg and Markus Gerhards, *Phys. Chem. Chem. Phys.*, 2010
DOI: 10.1039/c000424c

Probing the specific interactions and structures of gas-phase vancomycin antibiotics with cell-wall precursor through IRMPD spectroscopy
Jean Christophe Poully, Frédéric Lecomte, Nicolas Nieuwjaer, Bruno Manil, Jean Pierre Schermann, Charles Desfrançois, Florent Calvo and Gilles Grégoire, *Phys. Chem. Chem. Phys.*, 2010
DOI: 10.1039/b923787a

Two-dimensional network stability of nucleobases and amino acids on graphite under ambient conditions: adenine, L-serine and L-tyrosine
Ilko Bald, Sigrid Weigelt, Xiaojing Ma, Pengyang Xie, Ramesh Subramani, Mingdong Dong, Chen Wang, Wael Mamdouh, Jianguo Wang and Flemming Besenbacher, *Phys. Chem. Chem. Phys.*, 2010
DOI: 10.1039/b924098e

Importance of loop dynamics in the neocarzinostatin chromophore binding and release mechanisms
Bing Wang and Kenneth M. Merz Jr., *Phys. Chem. Chem. Phys.*, 2010
DOI: 10.1039/b924951f

Structural diversity of dimers of the Alzheimer Amyloid-(25-35) peptide and polymorphism of the resulting fibrils
Joan-Emma Shea, Andrew I. Jewett, Guanghong Wei, *Phys. Chem. Chem. Phys.*, 2010
DOI: 10.1039/c000755m

Two-dimensional network stability of nucleobases and amino acids on graphite under ambient conditions: adenine, L-serine and L-tyrosine†

Ilko Bald,[a] Sigrid Weigelt,[a] Xiaojing Ma,[a] Pengyang Xie,[b] Ramesh Subramani,[a] Mingdong Dong,[a] Chen Wang,[c] Wael Mamdouh,[a] Jianguo Wang[b] and Flemming Besenbacher*[a]

Received 17th November 2009, Accepted 5th March 2010
First published as an Advance Article on the web 9th March 2010
DOI: 10.1039/b924098e

We have investigated the stability of two-dimensional self-assembled molecular networks formed upon co-adsorption of the DNA base, adenine, with each of the amino acids, L-serine and L-tyrosine, on a highly oriented pyrolytic graphite (HOPG) surface by drop-casting from a water solution. L-serine and L-tyrosine were chosen as model systems due to their different interaction with the solvent molecules and the graphite substrate, which is reflected in a high and low solubility in water, respectively, compared with adenine. Combined scanning tunneling microscopy (STM) measurements and density functional theory (DFT) calculations show that the self-assembly process is mainly driven by the formation of strong adenine–adenine hydrogen bonds. We find that pure adenine networks are energetically more stable than networks built up of either pure L-serine, pure L-tyrosine or combinations of adenine with L-serine or L-tyrosine, and that only pure adenine networks are stable enough to be observable by STM under ambient conditions.

Introduction

Proteins are very important key elements in biological systems, and among their various functions they act as enzymes in the synthesis of living materials. The interaction of proteins with DNA underlies fundamental biological processes such as gene transcription,[1–4] DNA replication, and control of gene expression by DNA packaging in chromatin.[5,6] It is thus of great interest to investigate the interaction of the DNA nucleobases—the essential components of DNA/RNA—with amino acids, which are the building blocks of proteins.

Scanning tunneling microscopy (STM) is the technique of choice for studying molecule–molecule interactions at the atomic and molecular scale.[7–10] Extensive STM studies of single purine and pyrimidine bases and combinations thereof have been performed on a variety of substrates under both ambient and ultrahigh vacuum (UHV) conditions.[11–21] In particular, the nucleobase adenine (A), one of the purine bases, has been investigated in great detail on highly oriented pyrolytic graphite (HOPG) at both the air–solid and liquid (1-octanol)–solid interface, and it has been shown both experimentally and theoretically that A forms a homochiral and a heterochiral structure, both of which consist of rows of homochiral A dimers.[22–26] In contrast, amino acids have, to our knowledge, not been investigated by STM under ambient conditions,[27] only on more reactive surfaces under UHV conditions[28–31] and so far, only a few studies have aimed to investigate the interactions between amino acids and DNA bases by STM.[32] It is well known that molecules such as the DNA nucleobase guanine form self-assembled 2D networks on Au(111), but the structure changes significantly after annealing at 400 K in UHV.[17] The self-assembled structures are again different under ambient conditions in solution.[16] To obtain biologically relevant information about the interplay between proteins and DNA, it is important to carry out investigations on the interaction between nucleobases and amino acids under ambient conditions.

Through an interplay of ambient STM and theoretical density functional theory (DFT) investigations, we have studied the molecular networks formed on a HOPG surface upon adsorption and co-adsorption of the purine base, A, with two amino acids by drop-casting from a water solution. The stability of 2D ordered networks is determined by (i) the stabilization energy of the bare molecular networks, and (ii) the interplay of the adsorption energy with the solvent–molecule interactions that determine whether a physisorbed molecular network is formed during the incubation period. To study the involved interactions systematically, we chose one amino acid with higher solubility in water (L-serine (Ser), 4 M[33]) compared to that of A (7.23 mM[34]), and another amino acid with a comparably lower solubility in water (L-tyrosine (Tyr), 2.8 mM[35]). The solubility in water reflects the polarity of a molecule and its ability to form hydrogen bonds with

[a] *Interdisciplinary Nanoscience Center (iNANO), Centre for DNA Nanotecnology (CDNA), and Department of Physics and Astronomy, Aarhus University, 8000 Aarhus C, Denmark. E-mail: fbe@inano.au.dk; Fax: +4589423690; Tel: +4589423604*
[b] *College of Chemical Engineering and Materials Science, Zhejiang University of Technology, Hangzhou 310032, P. R. China. E-mail: jgw@zjut.edu.cn; Fax: +86 571 88871037; Tel: +86 571 88871037*
[c] *National Center for Nanoscience and Technology, Beijing 100190, P. R. China*

† Electronic supplementary information (ESI) available: Figs. S1–S5. See DOI: 10.1039/b924098e

surrounding water molecules. A lower solubility in water is basically expected to imply a stronger interaction with the non-polar graphite substrate, which promotes the formation of physisorbed self-assembled monolayers. In the present study the influence of (i) the stabilization energy due to intermolecular hydrogen bonding and (ii) the adsorption energy on the ability to form self-assembled monolayers is investigated.

Methods

STM experiments

The molecules, A (99%, Aldrich), Ser (>99.0%, Fluka), and Tyr (>99.0%, Fluka), were dissolved in Milli-Q water to yield 5 mM concentrations for A and Ser and a saturated 2.8 mM solution for Tyr. A droplet of 15–20 μL was deposited onto a freshly cleaved HOPG surface followed by incubation for 30 min at room temperature. After incubation the excess solution was removed by blow-drying with dry nitrogen gas, leaving a monolayer of adsorbed molecules. The STM experiments were performed in air at room temperature (21 ± 1 °C, Humidity 22%) using a Multimode SPM system with a Nanoscope IIIA controller (Veeco Instruments Inc., Santa Barbara, CA). The measurements were performed using mechanically cut Pt/Ir (80%/20%) STM tips. The molecular structures were typically scanned with bias voltages (V) between 400 mV and 1200 mV and tunneling currents (I) between 150 pA and 250 pA.

Calibration and drift compensation in the STM images was achieved by acquisition of a series of STM images of the molecular structures and the atomically resolved HOPG surface at the same spot and with the same scan speed. This was achieved by varying the bias voltage until we entered the STM manipulation regime where the molecular networks were destroyed/removed by the tip, and the underlying HOPG substrate was revealed.

All STM images were recorded in the constant current mode, and the STM images were subsequently analyzed using the Scanning Probe Image Processor (SPIP) software version 5.0.1 (Image Metrology ApS, Lyngby, Denmark). The correlation averaging method was used to display high-resolution STM images.

DFT calculations

The first-principles DFT calculations were performed both for gas-phase networks and for networks on the graphite surface with the DMol module in Materials Studio.[36,37] The generalized gradient approximation with the PW91 functional was used to describe the exchange–correlation effects.[38] In DMol the physical wave function is expanded on an accurate numerical basis set, and fast convergent 3D integration is used to calculate the matrix elements occurring in the Ritz variational method. In this study a double numerical basis set with polarization functions (DNP) and a real space cut-off of 5.0 Å was used. The sizes of the DNP basis sets are comparable with the 6-31G** basis and believed to be much more accurate than Gaussian basis sets of the same size. The k-point sampling was done by the use of the Monkhorst–Pack scheme, and the threshold of density matrix convergence was set to 10^{-6}.

The stability of the gas-phase structures was evaluated by the network stabilization energy E_g, defined by:

$$E_g = nE_{Ade} + mE_{Ser/Tvr} - E_{nAde+m(Ser/Tvr)}$$

The binding energy, E_s, of the molecules or networks on the graphite surface is defined by:

$$E_s = nE_{Ade} + mE_{Ser/Tvr} + E_{Gra} - E_{nAde+m(Ser/Tvr)+Gra}$$

Results and discussion

Characterisation of pure adenine networks

STM investigations of the HOPG surface covered with 5 mM aqueous solutions of pure A following removal of excess solution reveal the formation of a complete A monolayer. In contrast, a similar treatment with each of the amino acids solutions, Ser and Tyr, does not leave any sign of the formation of stable amino acid structures upon imaging with the STM in air. Instead the clean HOPG surface is revealed in those cases.

In Fig. 1 STM images of the pure A structures are depicted. Large-scale images (see Fig. 1a and Fig. S1 of the ESI†) show that the molecules are arranged into striped domains with the stripes oriented perpendicular to the high-symmetry directions of the underlying atomic HOPG lattice, indicating a directional interaction between the HOPG surface and the A molecules. In accordance with previous studies[22–26] of A adsorbed on HOPG by other preparation procedures, we find two different adsorption structures, in the following referred to as the A structure and the B structure, respectively as displayed in Fig. 1. Inspection of the structures at a large scale (Fig. 1a) reveals that the contrast between neighbouring rows is more pronounced in domains with a B structure than in domains with an A structure. A zoom-in on the domains (Fig. 1b–d) shows that the rows are built up of homochiral A dimers (Fig. 1e). In the A structure (Fig. 1b and c) all rows consist of dimers with the same chirality, which renders the A structure homochiral. In contrast to that in the B structure, adjacent rows consist of dimers with opposite chirality (see Fig. 1d), which renders the B structure overall heterochiral. In the figures, low-energy molecular network structures that resulted from DFT calculations are superimposed on the STM images.

Even under very gentle scanning conditions (I = 180–200 pA and V = 0.8–1.2 V), we often observe that the scanned domain is removed after a few scans due to strong interactions with the tip, and we find that even if only a small portion of an area is scanned, the collapse/disappearance of the molecular structure is transferred to the complete domain, as seen in the zoom-out image in Fig. S1 of the ESI.† By decreasing the bias voltage below 400 mV, we could trigger the collapse of the domains whereby atomic-scale images of the underlying substrate could be obtained. In this way, drift-corrected measurements of the A unit cells with very high accuracy could be obtained. From an image sequence of four (six) images at the same spot, we find unit cell dimensions of the A (B) domains to be a = 1.14 ± 0.03 nm (2.38 ± 0.07 nm), b = 0.86 ± 0.03 nm (0.84 ± 0.03 nm) and ϕ = 70.0 ± 2.1° (69.8 ± 2.2°)

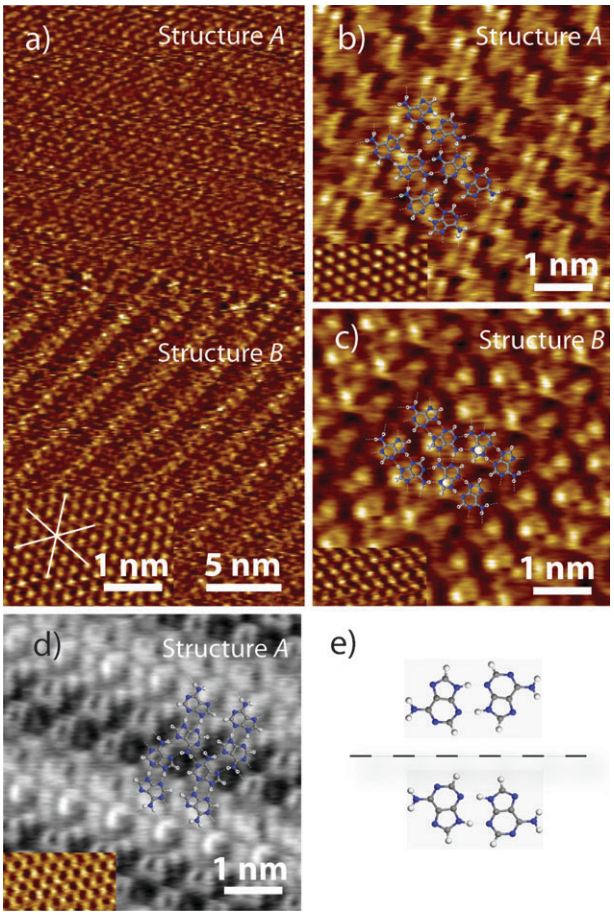

Fig. 1 Adenine on HOPG deposited from a 5 mM aqueous adenine solution. Insets show the graphite substrate that was recorded for calibration subsequent to the respective adenine imaging. Theoretically predicted network structures of adenine are superimposed on high-resolution images. (a) Large-scale image displaying a domain boundary between a homochiral *A* and a heterochiral *B* structure; $I = 200$ pA, $V = 1000$ mV (HOPG: $I = 517$ pA, $V = 350$ mV). (b) Zoom-in on a domain composed of the *A* structure; $I = 200$ pA, $V = 700$ mV (HOPG: $I = 467$ pA, $V = 296$ mV). (c) Zoom-in on a domain composed of the *B* structure; $I = 200$ pA, $V = 1100$ mV (HOPG: $I = 517$ pA, $V = 350$ mV). (d) Inverted image of an *A* structure; $I = 183$ pA, $V = 600$ mV (HOPG: $I = 713$ pA, $V = 231$ mV). (e) The two chiral forms of adenine dimers. Structure *A* is built up of one type of dimer, whereas structure *B* consists of both enantiomeric dimers.

respectively. These measurements fit well with the gas-phase DFT results,[23] $a = 1.14$ nm (2.38 nm), $b = 0.86$ nm (0.85 nm) and $\phi = 73.7°$ (69.0°) for the *A* (*B*) domains and are of a significantly higher accuracy than previous measurements of the unit cell parameters under 1-octanol conditions.[23]

Depending on the STM tip, the scan direction[18] and the tunneling conditions, the appearance of the molecular structures is observed to change dramatically.[39–41] In Fig. 2 a series of STM images of the same heterochiral A domain obtained at different bias voltages is displayed, indicating a strong bias dependence of the appearance of the A network. As seen, adjacent rows are often imaged at different contrast resulting in varying STM patterns. One might conclude at first sight that the networks were composed of not just A molecules. Images recorded at high bias ($V > 700$ mV)

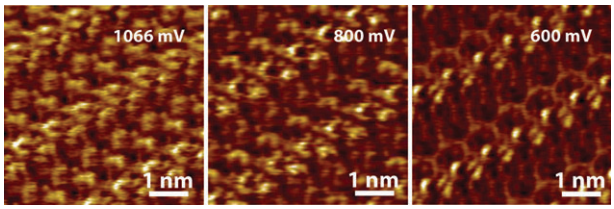

Fig. 2 Bias-dependent sequence of STM images of the heterochiral adenine structure. All the images are obtained at the same location with a current set-point $I = 200$ pA.

are often easier to interpret than images at lower bias, since the triangular shape of the A molecules is often found at high bias, whereas low-bias images only show parts of the molecules mixed with contributions from the underlying HOPG surface. For instance, Fig. 1c shows that the amino group and the two parts of the purine ring (the pyrimidine ring and the imidazole ring) of a single molecule can be clearly distinguished, and also the network of hydrogen bonds appears in the STM image.

Furthermore, we sometimes find that the molecules are imaged as depressions instead of protrusions. An example of an STM image of the homochiral *A* domain obtained in such an inverted-tip imaging mode in which the molecules appear dark instead of bright is displayed in Fig. 1d. To help the reader, the colour scale has been inverted by the image processing software. In such inverted images, single molecules are often easier to distinguish than in images obtained in the conventional non-inverted mode.

Co-deposition of adenine with L-serine/L-tyrosine

Fig. 3 shows a collection of STM images of the molecular networks formed on an HOPG surface after incubation of the substrate in an aqueous solution containing 5 mM A and 5 mM Ser/Tyr respectively for 30 min following blow-drying with nitrogen. A thorough inspection of several samples at different STM biases and under different imaging conditions (see Figs. S2 and S3 of the ESI†) revealed that all the stable molecular structures consist exclusively of A molecules, and no signs of any new co-adsorption structures are revealed. In all cases we find both homochiral *A* domains (Fig. 3b and e) and heterochiral *B* domains (Fig. 3c and f) on the HOPG surface. Measurements of the unit cells formed upon A-Ser (A-Tyr) sample treatment yield $a = 1.18 \pm 0.03$ nm, $b = 0.82 \pm 0.04$ nm and $\phi = 70.2 \pm 2.1°$ ($a = 1.07 \pm 0.06$ nm, $b = 0.84 \pm 0.03$ nm, $\phi = 70 \pm 3°$) for the homochiral *A* structures and $a = 2.38 \pm 0.07$ nm, $b = 0.85 \pm 0.03$ nm and $\phi = 69.9 \pm 2.1°$ ($a = 2.36 \pm 0.03$ nm, $b = 0.87 \pm 0.01$ nm, $\phi = 65 \pm 2°$) for the heterochiral *B* structures. This is in good agreement both with the numbers obtained from the DFT calculations and observed in the measurements of the pure A samples. Sometimes small highly unstable structures are also found on the surface. However, such domains could also be found on samples treated only with A. We therefore conclude that only stable A networks are formed, whereas the amino acids remain dissolved in solution.

To further elucidate these findings, gas-phase DFT calcualtions for molecular dimers and networks were performed (see Fig. 4 and 5 and Figs. S4 and S5 of the ESI†).

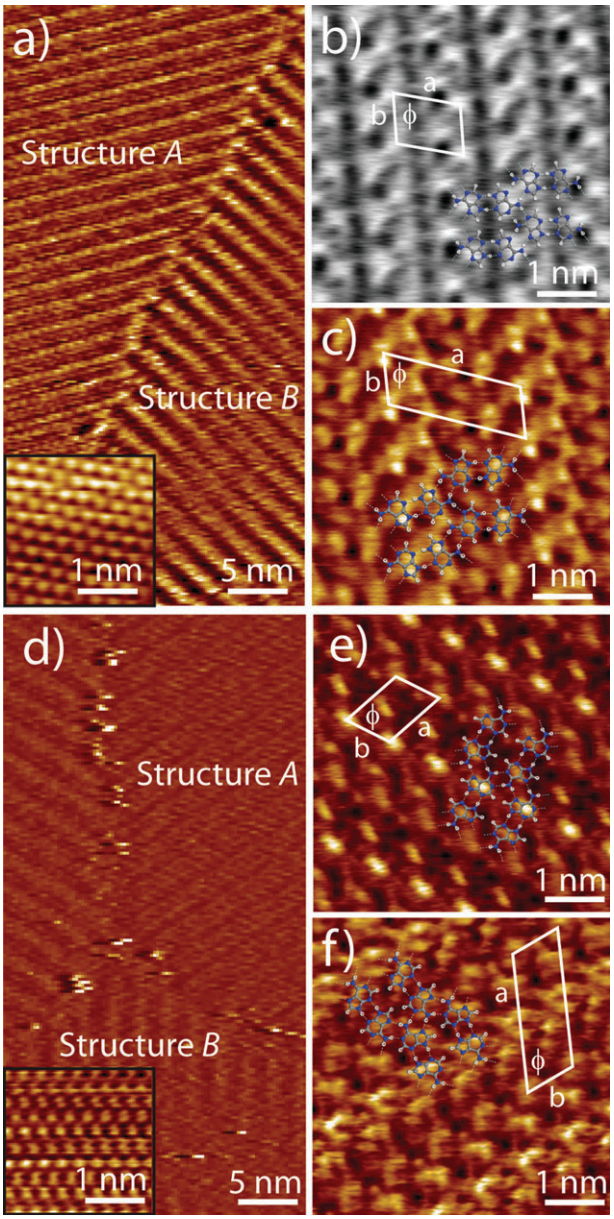

Fig. 3 Co-adsorption of adenine with L-serine (a–c) and with L-tyrosine (d–f). In both cases only pure adenine domains are found. (a, d) Large-scale current STM images showing neighboring homochiral *A* and heterochiral *B* domains. Note that the image in (d) is obtained in the inverted imaging mode (the unprocessed image can be seen in Fig. S2a of the ESI†). (b, e) Zoom-in on homochiral *A* domains. The STM image in b) was obtained in the inverted imaging mode. (c, f) Zoom-in on heterochiral *B* domains. Imaging parameters: (a) I = 284 pA, V = 825 mV (HOPG: I = 511 pA, V = 563 mV); (b) I = 200 pA, V = 800 mV; (c) I = 190 pA, V = 900 mV; (d) I = 200 pA, V = 800 mV (HOPG: I = 927 pA, V = 415 mV); (e) I = 343 pA, V = 700 mV; (f) I = 200 pA, V = 1066 mV.

Fig. 4a–c shows the structure and stabilization energy of the most stable homodimers of A, Ser and Tyr, which all exhibit two intermolecular hydrogen bonds. Of all three species, the A dimer is the most stable complex due to strong NH···N hydrogen bonds. For the binding of the two amino acids to A several possibilities for hydrogen bonding exist, the most

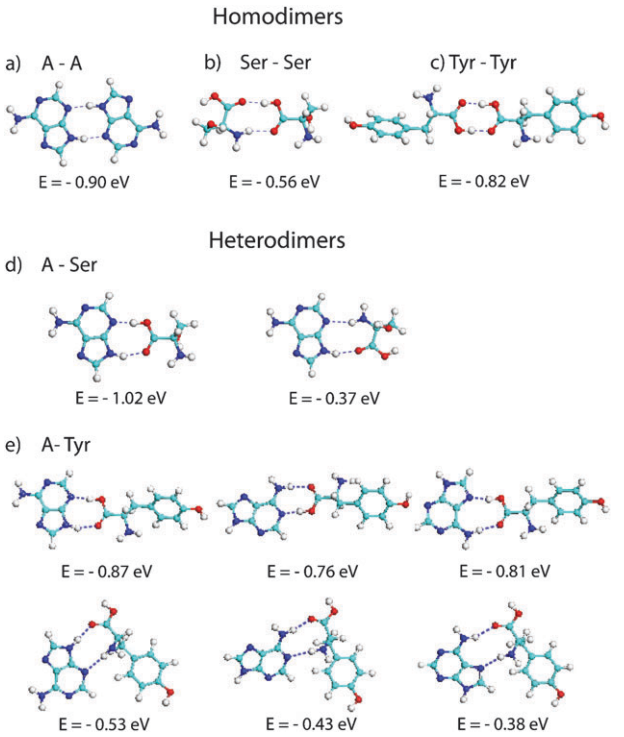

Fig. 4 (a–c) Structures and stabilization energies of homodimers of adenine, L-serine and L-tyrosine resulting from DFT calculations; (d, e) Calculated structures and stabilization energies of heterodimers of A and Tyr, and A and Ser.

relevant of which are displayed in Fig. 4d and e. The calculations show that the most stable heterodimers are formed by intermolecular hydrogen bonding of the carboxylic group of the amino acids with N1 and N9–H of the A molecule. The stabilization energy of these heterodimers (1.02 eV for Ser, and 0.87 eV for Tyr) is similar to the stabilization energy of the A dimer (0.90 eV). However, the situation changes when considering 2D network structures. In Fig. 5 the structures and stabilization energies (per four molecules) of A networks and intermixed networks comprised of A and Ser respectively Tyr are depicted. The most stable intermixed structures were found to consist of consecutive rows of A and amino acid dimers (Fig. 5b and c), respectively, having stabilization energies of 3.46 eV and 2.97 eV, respectively. In comparison, calculations of the homochiral and heterochiral A structures (Fig. 5a) yield stabilization energies of 3.84 eV and 3.87 eV respectively, as also found in previous studies.[23,42] The higher stability of A networks is a consequence of the larger number of intermolecular hydrogen bonds that are formed compared to intermixed networks.

The formation of 2D self-assembled nanostructures is not only governed by molecule–molecule interactions, but also by molecule–surface interactions. To reveal the influence of the adsorption energy on the ability of A, Ser and Tyr to form self-assembled monolayers on graphite we conducted DFT calculations on adsorbed molecules and molecular networks. In Fig. 6 structures of the single A, Ser and Tyr molecules and the most stable network structures adsorbed on graphite as calculated with DFT are displayed. The results show that a

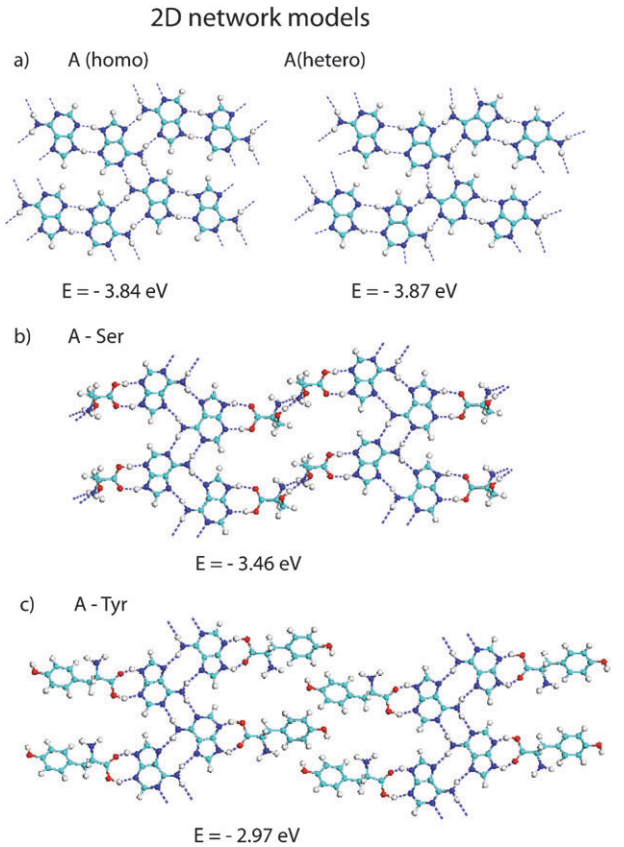

Fig. 5 Structures and stabilization energies (per 4 molecules) of the 2D molecular networks resulting from DFT calculations. (a) Homochiral and heterochiral A networks, (b, c) mixed A-Ser/Tyr networks. For the intermixed structures only the most stable networks are displayed.

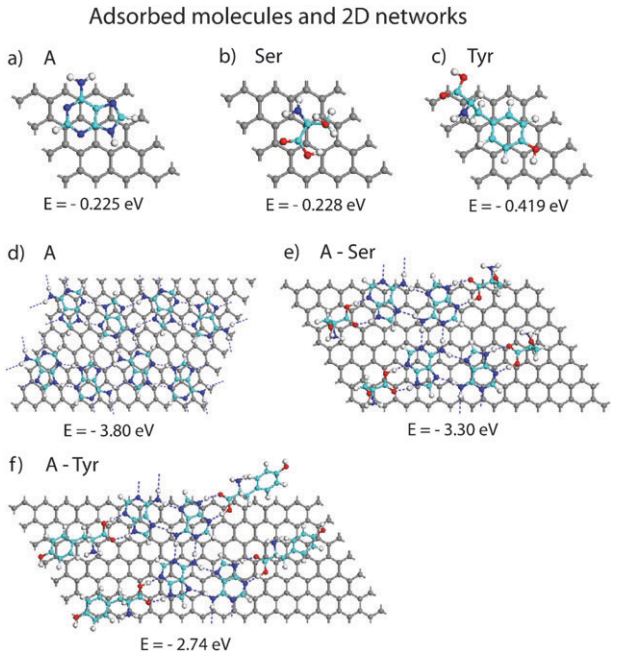

Fig. 6 DFT calculations of molecules adsorbed on graphite. Stabilization energies for a single (a) adenine, (b) L-serine,and (c) L-tyrosine molecule on HOPG. Structures and stabilization energies (per 4 molecules) on HOPG for (d) the homochiral adenine network, (e) the intermixed adenine-L-serine network and (f) the intermixed adenine-L-tyrosine network.

single Tyr possesses the highest adsorption energy (0.419 eV) compared to A (0.225 eV) and Ser (0.228 eV). In accordance with other studies[43,44] this is caused by attractive π–π interactions between the benzene ring of Tyr and the HOPG surface. Since we observed the formation of A self-assembled monolayers the calculated adsorption energies of A, Ser and Tyr indicate that also the interaction of the amino acids with the graphite surface is basically large enough to render the formation of intermixed A/amino acid networks feasible. However, DFT calculations of molecular networks adsorbed on the graphite (Fig. 6d–f) reveal that adsorbed A networks are considerably more stable than intermixed networks. A comparison of the network stabilization energies in the gas phase (Fig. 5) with the adsorbed state (Fig. 6) suggests that the molecule–substrate interactions are very small compared to the intermolecular interactions. This is also evident from the molecule–substrate distance, which increases from 0.23 nm for the single adsorbed molecules to 0.42 nm for the molecular networks. The driving force for formation of nucleobase/amino acid self-assembled monolayers on the HOPG surface is thus the stabilization energy of the molecular networks.

The DFT calculations and experimental findings reveal that the formation of hydrogen bonded self-assembled monolayers under ambient conditions requires a large network stabilization energy, and in the case of graphite the substrate only acts as a template. Despite strong hydrogen bonding between A and Tyr and a high adsorption energy of Tyr on graphite no intermixed networks can be observed due to a low total network stabilization energy.

Gas-phase DFT calculations and STM measurements were also performed on a range of samples incubated with aqueous solutions of A combined with other amino acids. In no cases did we find clear evidence of the formation of intermixed co-adsorbed networks.

Conclusions

The formation of 2D molecular nanostructures is governed by a complex interplay between molecule–molecule and molecule–surface interactions. STM experiments and DFT calculations reveal that pure A networks are energetically more favourable than networks built up of either Ser, Tyr or combinations of A with Ser or Tyr. Our theoretical results suggest that the interaction of the self-assembled molecular network with a graphite surface is rather small compared to the intermolecular interactions. The amino acids Ser and Tyr can form strong hydrogen bonds with the nucleobase A (close to 1 eV binding energy), however, the total number of hydrogen bonds in a 2D intermixed network is smaller than in pure A networks. A comparatively strong binding of Tyr to graphite is not sufficient to form stable intermixed A-Tyr networks under ambient conditions. This implies that a sample incubated in a solution containing an excess of A molecules would be covered only by homomolecular A networks. The present results suggest that the interaction between amino acids and nucleobases in true biological processes might require 3D conformations for molecular recognition.

Acknowledgements

We acknowledge financial support from the Villum Kann Rasmussen Foundation (SW and MD), the Deusche Forschungsgemeinschaft (IB), and the Danish National Research Foundation (WM). Furthermore, we thank the Danish Natural Science Research Council and the Danish Ministry for Science and Innovation for support to iNANO, and the Carlsberg Foundation and the Danish National Research Foundation for support to CDNA.

References

1 J. D. Watson and F. H. C. Crick, *Nature*, 1953, **171**, 964–967.
2 R. D. Kornberg, *Proc. Natl. Acad. Sci. U. S. A.*, 2007, **104**, 12955–12961.
3 F. Crick, *Nature*, 1970, **227**, 561–563.
4 P. Nissen, J. Hansen, N. Ban, P. B. Moore and T. A. Steitz, *Science*, 2000, **289**, 920–930.
5 T. J. Richmond and C. A. Davey, *Nature*, 2003, **423**, 145–150.
6 N. Dillon, *Chromosome Res.*, 2006, **14**, 117–126.
7 S. De Feyter and F. C. De Schryver, *Chem. Soc. Rev.*, 2003, **32**, 139–150.
8 J. V. Barth, G. Costantini and K. Kern, *Nature*, 2005, **437**, 671–679.
9 A. Schiffrin, A. Riemann, W. Auwarter, Y. Pennec, A. Weber-Bargioni, D. Cvetko, A. Cossaro, M. Alberto and J. V. Barth, *Proc. Natl. Acad. Sci. U. S. A.*, 2007, **104**, 5279–5284.
10 J. Elemans, S. B. Lei and S. De Feyter, *Angew. Chem., Int. Ed.*, 2009, **48**, 7298–7332.
11 T. Boland and B. D. Ratner, *Langmuir*, 1994, **10**, 3845–3852.
12 M. Kasaya, H. Tabata and T. Kawai, 13th International Vacuum Congress / 9th International Conference on Solid Surfaces (IVC-13/ICSS-9), Yokohama, Japan, 1995.
13 R. E. A. Kelly, M. Lukas, L. N. Kantorovich, R. Otero, W. Xu, M. Mura, E. Laegsgaard, I. Stensgaard and F. Besenbacher, *J. Chem. Phys.*, 2008, **129**, 184707.
14 M. Lukas, R. E. A. Kelly, L. N. Kantorovich, R. Otero, W. Xu, E. Laegsgaard, I. Stensgaard and F. Besenbacher, *J. Chem. Phys.*, 2009, **130**, 024705–024709.
15 W. Mamdouh, M. D. Dong, S. L. Xu, E. Rauls and F. Besenbacher, *J. Am. Chem. Soc.*, 2006, **128**, 13305–13311.
16 W. Mamdouh, R. E. A. Kelly, M. D. Dong, L. N. Kantorovich and F. Besenbacher, *J. Am. Chem. Soc.*, 2008, **130**, 695–702.
17 R. Otero, M. Schock, L. M. Molina, E. Laegsgaard, I. Stensgaard, B. Hammer and F. Besenbacher, *Angew. Chem., Int. Ed.*, 2005, **44**, 2270–2275.
18 S. J. Sowerby, M. Edelwirth, M. Reiter and W. M. Heckl, *Langmuir*, 1998, **14**, 5195–5202.
19 S. J. Sowerby and G. B. Petersen, *J. Electroanal. Chem.*, 1997, **433**, 85–90.
20 S. J. Sowerby, P. A. Stockwell, W. M. Heckl and G. B. Petersen, *Origins Life Evol. Biosphere*, 2000, **30**, 81–99.
21 N. J. Tao, J. A. Derose and S. M. Lindsay, *J. Phys. Chem.*, 1993, **97**, 910–919.
22 J. E. Freund, M. Edelwirth, P. Krobel and W. M. Heckl, *Phys. Rev. B: Condens. Matter*, 1997, **55**, 5394–5397.
23 W. Mamdouh, M. D. Dong, R. E. A. Kelly, L. N. Kantorovich and F. Besenbacher, *J. Phys. Chem. B*, 2007, **111**, 12048–12052.
24 H. Ou-yang, R. A. Marcus and B. Källebring, *J. Chem. Phys.*, 1994, **100**, 7814–7824.
25 S. J. Sowerby, M. Edelwirth and W. M. Heckl, *J. Phys. Chem. B*, 1998, **102**, 5914–5922.
26 N. J. Tao and Z. Shi, *J. Phys. Chem.*, 1994, **98**, 1464–1471.
27 S. J. Sowerby, G. B. Petersen and N. G. Holm, *Origins Life Evol. Biosphere*, 2002, **32**, 35–46.
28 V. Humblot, C. Methivier, R. Raval and C. M. Pradier, 24th European Conference on Surface Science (ECOSS-24), Paris, France, 2006.
29 A. Kühnle, T. R. Linderoth, B. Hammer and F. Besenbacher, *Nature*, 2002, **415**, 891–893.
30 M. Lingenfelder, G. Tomba, G. Costantini, L. C. Ciacchi, A. De Vita and K. Kern, *Angew. Chem., Int. Ed.*, 2007, **46**, 4492–4495.
31 M. Forster, M. S. Dyer, M. Persson and R. Raval, *J. Am. Chem. Soc.*, 2009, **131**, 10173–10181.
32 Q. Chen and N. V. Richardson, *Nat. Mater.*, 2003, **2**, 324–328.
33 H.-C. Tseng, C.-Y. Lee, W.-L. Weng and I. M. Shiah, *Fluid Phase Equilib.*, 2009, **285**, 90–95.
34 J. Krzaczkowska, J. Gierszewski and G. Slosarek, *J. Solution Chem.*, 2004, **33**, 395–404.
35 R. Carta and G. Tola, *J. Chem. Eng. Data*, 1996, **41**, 414–417.
36 B. Delley, *J. Chem. Phys.*, 1990, **92**, 508–517.
37 B. Delley, *J. Chem. Phys.*, 2000, **113**, 7756–7764.
38 J. P. Perdew and Y. Wang, *Phys. Rev. B: Condens. Matter*, 1992, **45**, 13244–13249.
39 H. Gawronski, J. Henzi, V. Simic-Milosevic and K. Morgenstern, *Appl. Surf. Sci.*, 2007, **253**, 9047–9053.
40 J. A. Nieminen, E. Niemi and K. H. Rieder, *Surf. Sci.*, 2004, **552**, L47–L52.
41 E. Shapir, J. Y. Yi, H. Cohen, A. B. Kotlyar, G. Cuniberti and D. Porath, *J. Phys. Chem. B*, 2005, **109**, 14270–14274.
42 R. E. A. Kelly and L. N. Kantorovich, *Surf. Sci.*, 2005, **589**, 139–152.
43 S. M. Tomásio and T. R. Walsh, *J. Phys. Chem. C*, 2009, **113**, 8778–8785.
44 H. Xie, E. J. Becraft, R. H. Baughman, A. B. Dalton and G. R. Dieckmann, *J. Pept. Sci.*, 2008, **14**, 139–151.